



Research Article

Effects of different surfactants on morphology of TiO₂ and Zr-doped TiO₂ nanoparticles and their applications in MB dye photocatalytic degradation

M. Mahdi Honarmand¹ · M. Emami Mehr²  · Mohadeseh Yarahmadi² · M. Hossein Siadati²

© Springer Nature Switzerland AG 2019

Abstract

In recent years, great attention has been paid to the synthesis of nano-size TiO₂ due to its wide range of applications, particularly in the area of degradation of organic pollutants. In this study, different surfactants were used in synthesizing TiO₂ and Zr-doped TiO₂ nanoparticles. The effects of the surfactants' types and concentrations on the morphology and size of the TiO₂ nanoparticles were studied. The synthesized nanoparticles were characterized using Fourier transform infrared spectroscopy, X-ray diffraction, scanning electron microscopy (SEM), energy-dispersive X-ray spectroscopy, and transmission electron microscopy. It was found that the TiO₂ nanoparticles are a mixture of two anatase and rutile phases, whereas the surfactant-modified TiO₂ nanoparticles have a dominant anatase phase. According to the SEM images, the synthesized nanoparticles' morphologies depended not only on the type, but also on the concentration of the surfactants. The photocatalytic behavior of the nanoparticles on the degradation of methylene blue (MB) dye was evaluated. The maximum efficiency was achieved for the TiO₂ nanoparticles synthesized using 0.08 molar surfactant Sodium bis(2-ethylhexyl)sulfosuccinate; reached 76% after 300 min of ultraviolet radiation. This indicated superior photocatalytic activity of this sample compared to all other synthesized nanoparticles, due to its uniform spherical morphology and particle sizes of 40–50 nm. For this sample, the effects of such parameters as catalyst amount and MB dye solution pH and temperature were optimized for its photocatalytic activity.

Keywords TiO₂ · Zr-doped TiO₂ · Surfactants · Microemulsion method · Photocatalytic activity · Methylene blue

1 Introduction

In the past decades, much efforts have gone into expanding the photocatalytic systems in which transition metal semiconductors are used [1–3]. In recent years, due to its chemical stability, nontoxicity, inexpensiveness, and high efficiency [4, 5], great attention has been paid to the synthesis of nanoparticle TiO₂ due to its wide range of applications in sensors, pigments, sunblock creams, fuel cells, catalysts and photocatalysts [6–8]. Among the different uses of TiO₂, its photocatalytic application for the degradation of organic pollutants has significantly increased [9, 10]. TiO₂ has three crystalline phases of anatase, rutile,

and brookite. Although the rutile crystalline phase is the most common crystalline structure of TiO₂ found in nature, the anatase crystalline phase with the band gap energy of 3.2 eV shows a better photocatalytic activity than the other two forms [11]. One of the problems of TiO₂ for photocatalytic applications is the high rate of electron-hole recombination on its surface, which reduces the photocatalytic efficiency of this photocatalyst [12]. Different factors such as dopant(s), oxidants, and various surfactants have been found to improve the photocatalytic behavior of TiO₂ nanoparticles [13–15]. Numerous studies have been conducted to show the effects of various surfactants and transition metals (e.g., iron, vanadium, copper, niobium, and

✉ M. Emami Mehr, emamimehr.m@email.kntu.ac.ir | ¹Faculty of Chemistry, K. N. Toosi University of Technology, Tehran, Iran. ²Faculty of Material Science and Engineering, K. N. Toosi University of Technology, Tehran, Iran.



cobalt) as dopants in improving its photocatalytic activity [16–21]. Doping TiO_2 with slight amounts of transition elements causes trapping of the electrons, which results in narrowing of the band gap and lowering electron-hole recombination. This creates intra-band states close to the valence band edges inducing visible-light absorption at sub-band-gap energies and thus enhancing its photocatalytic activity [22, 23]. In 2016, Fu et al. [24] reported that B, Zr and Co-doping effectively improved the visible light absorption of TiO_2 and thus enhanced its dye photocatalytic degradation.

Among the most widely used methods for preparation of TiO_2 nanoparticles are sol–gel, hydrothermal, solvothermal, and co-precipitation [25–28]. However, increasing attention recently has been paid to the use of microemulsion for the synthesis of TiO_2 nanoparticles [29]. If a chemical substance called surfactant (i.e., the surface-active agent) is added to the mixture of oil and water, then a microemulsion system is formed. Surfactants considerably decrease the water–oil interfacial tension by adsorbing at the interface of the two phases. Surfactants are amphiphilic molecules, which are comprised of a hydrophilic part (i.e., a polar head group) and a hydrophobic part (i.e., a nonpolar tail group), and are usually classified into four classes of cationic, anionic, nonionic, and zwitterionic based on their polar heads' load [30]. Since controlling the shape and size of TiO_2 nanoparticles depends on the type of surfactants [13], by paralleling the hydrophilic/lipophilic parts and geometry of surfactants, an appropriate surfactant can be selected.

In this study, the aim was to use microemulsion method to synthesize TiO_2 and Zr-doped TiO_2 nanoparticles and investigate the impacts of different surfactants on the morphology and size of the nanoparticles synthesized. For investigation of the photocatalytic degradation efficiency of the synthesized nanoparticles and comparison of their photocatalytic activities, the methylene blue dye pollutant was used. Furthermore, effects of such factors as catalyst amount, pH and temperature of the dye solution were optimized for the best synthesized catalyst.

In this paper the effects of different types of surfactants including anionic (AOT), cationic (TBAB) and nonionic (TX-100) on the shape and size of TiO_2 and Zr-doped TiO_2 nanoparticles were studied.

2 Materials

$\text{Ti}(\text{OMe})_4$ (95%, Sigma Aldrich) and $\text{Zr}(\text{acac})_4$ (99%, Merck) were used as precursors of titanium and zirconium, respectively. Sodium bis(2-ethylhexyl)sulfosuccinate, AOT (96%, Acros Organics), tetra-n-butylammonium bromide, TBAB (98% Sigma Aldrich), and polyoxyethylene

tert-octylphenyl, TX-100 (99%, Chem-Lab) were employed as anionic, cationic, and nonionic surfactants, respectively. Furthermore, deionized water, methylene blue dye (99% Sigma Aldrich), ammonium solution (28% Loba Chemie), ethanol (99% Merck), butanol (99% Rankem), and acetone (99% Merck) were utilized.

3 Characterization

FTIR spectra were recorded using the ABB-M330 spectrometer, Model FTLA 200-100, in the range of 400–4000 at the transition state. X-ray diffraction (XRD) analysis was carried out using a Philips device, Model 1730 PW. This device uses Cu-K α covered with nickel as its source of irradiation. Moreover, the diffracted X-ray in this device was measured at a wavelength of 1.542 Å and with the scanning speed of 2°/min. Surface morphologies of all synthesized samples were characterized using SEM, Model VEGA3 (Czech Republic) at a voltage of 20 kV. Energy dispersive X-ray (EDS) analysis was obtained using SEM, Model VEGA3 (Czech Republic), for identification of Zr content in all samples doped with TiO_2 . The size and the morphology of all synthesized samples were characterized using TEM, Model EM 208 S manufactured by Czech Republic, at a voltage of 100 kV. In order to track the degradation trend of the pollutant and to show how its concentration decreases, a Camspect UV–Vis spectrometer, Model M330, was adopted.

4 Synthesis

For synthesizing TiO_2 and Zr-doped TiO_2 nanoparticles, three kinds of surfactants were used; anionic AOT (sodium bis(2-ethylhexyl) sulfosuccinate), nonionic TX-100 (polyoxyethylene tert-octylphenyl or Triton X-100), and cationic TBAB (tetra-n-butylammonium bromide). Eight samples were synthesized and their names and specifications are shown in Table 1.

4.1 Synthesis of TiO_2 nanoparticles

For the synthesis of TiO_2 nanoparticles, 0.38 mmol of $\text{Ti}(\text{OMe})_4$ and 10 mL of ethanol were poured in a volumetric flask and stirred. In order to separate the phases, the solution was washed with ethanol. Then, the solution was centrifuged and the resultant precipitate was heated in an oven at 70 °C for 12 h to remove solvents. After that, the sample was heated in an electric furnace at 500 °C for 4 h, and subsequently the nanoparticles were obtained.

Table 1 Names and Specifications of the synthesized samples

Name	Sample/surfactant	Doped	Surfactant concentration
TiO ₂	TiO ₂	–	–
T/AOT	TiO ₂ /AOT	–	0.15
T/AOT-0.08	TiO ₂ /AOT	–	0.08
T/TX100	TiO ₂ /TX-100	–	0.15
T/TBAB	TiO ₂ /TBAB	–	0.15
Z/T/AOT	Zr/TiO ₂ /AOT	Or	0.15
Z/T/TX100	Zr/TiO ₂ /TX-100	Or	0.15
Z/T/TBAB	Zr/TiO ₂ /TBAB	Or	0.15

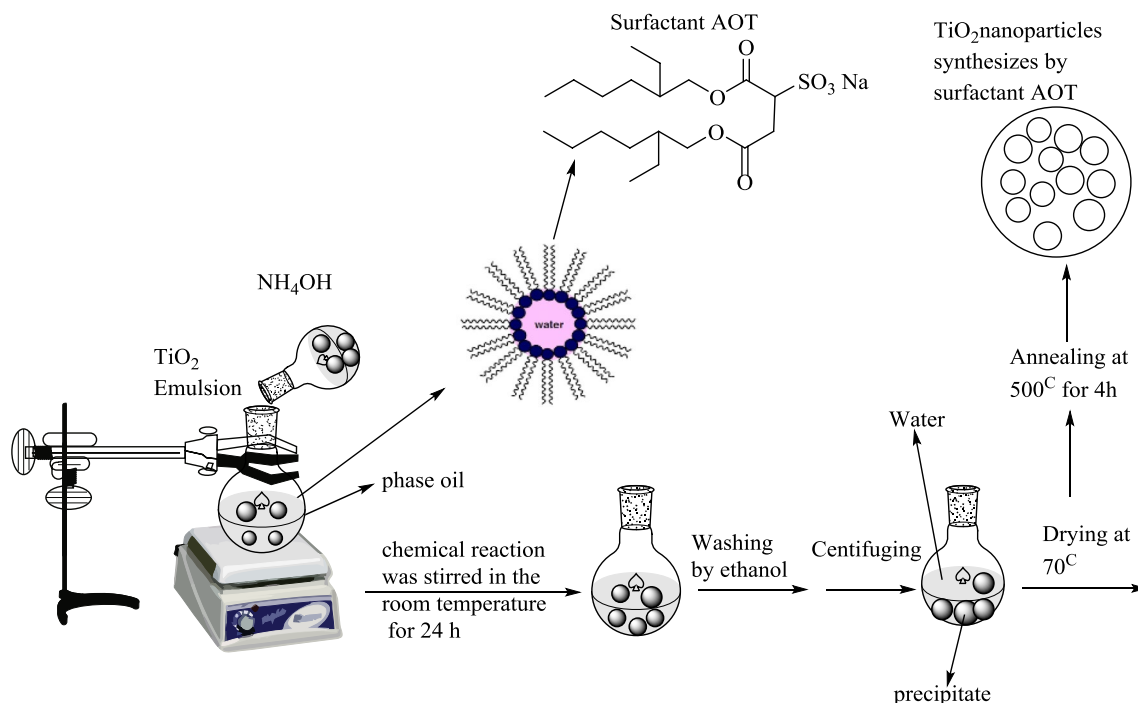
4.2 Synthesis of T/AOT nanoparticles

For the synthesis of T/AOT nanoparticles, two microemulsions, one containing 0.38 mmol of Ti(OMe)₄, 0.08 molar of AOT, and a few drops of butanol (microemulsion A) and the other containing 2.88 mmol of NH₄OH, 0.08 molar of surfactant, and a few drops of butanol (microemulsion B) were produced. While microemulsion A was being stirred, microemulsion B was added to it drop by drop. Then, the solution was stirred for 24 h. For separation of the phases, the solution was washed with ethanol. Subsequently, the solution was centrifuged and the resulting precipitate was heated in an oven at 70 °C for

12 h. Finally, the sample was placed in an electric furnace at 500 °C for 4 h to obtain the nanoparticles desired. Similarly, T/AOT-0.08, T/TX100, and T/TBAB nanoparticles were synthesized. Figure 1 presents the steps involved in the synthesis of the T/AOT nanoparticles.

4.3 Synthesis of Z/T/AOT nanoparticles

For the synthesis of Z/T/AOT nanoparticles, three microemulsions with different aqueous phases were prepared; 0.38 mmol of Ti(OMe)₄ (microemulsion A), 0.19 mmol of Zr(acac)₄ (microemulsion B), and 2.88 mmol of NH₄OH (microemulsion C). Each microemulsion contained 0.15 molar of AOT and about 5 ml of butanol. The two microemulsions A and B were mixed together to form microemulsion AB. After microemulsion AB was stirred for 1 h, microemulsion C was added to it dropwise, and then the solution was stirred for 24 h. Subsequently, in order to separate phases and remove organic compounds, the solution was washed with ethanol. The washed solution was then centrifuged and heated in an oven at 70 °C for 12 h. Then, the dried sample was annealed in an electric furnace at 500 °C for 4 h, and thus the nanoparticles were produced. Similarly, Z/T/TX100 and Z/T/TBAB nanoparticles were synthesized. Figure 2 presents the steps involved in the synthesis of the Z/T/AOT nanoparticles.

**Fig. 1** Representation of the T/AOT nanoparticles synthesis route via microemulsion

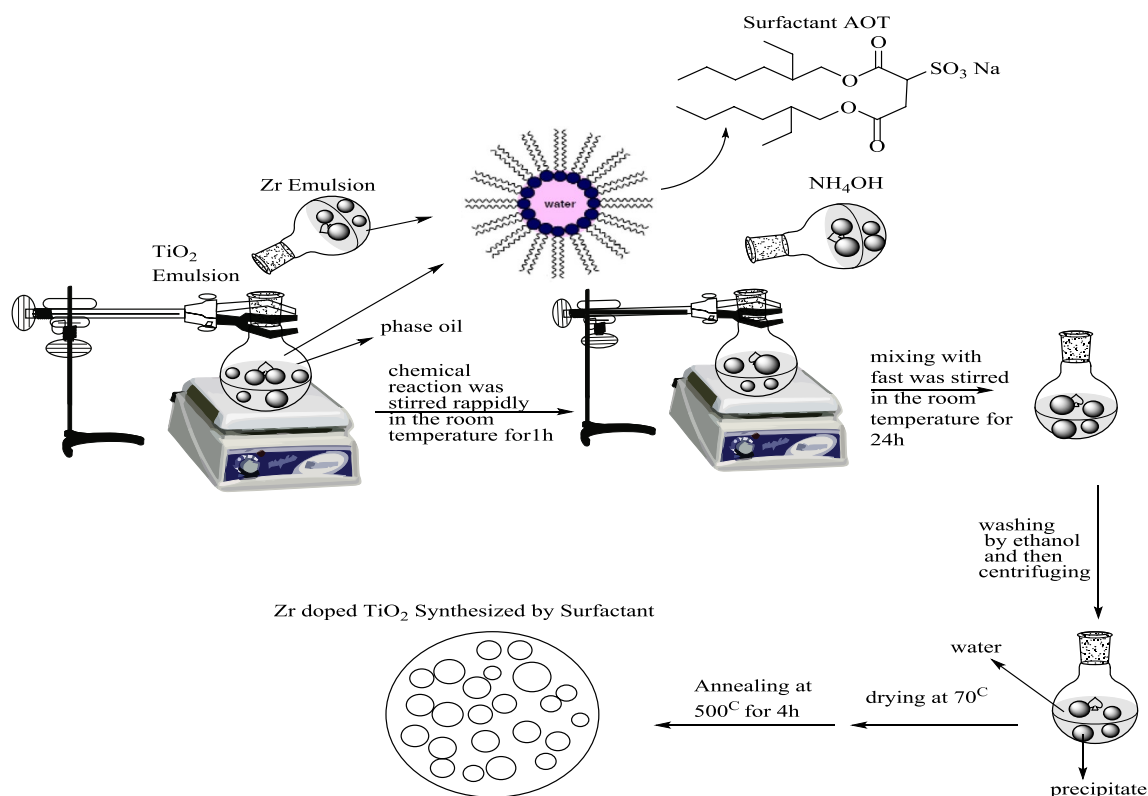


Fig. 2 Representation of the Zr/AOT nanoparticles synthesis route via microemulsion

5 Results and discussion

5.1 SEM investigation

5.1.1 Effects of surfactants on TiO₂ nanoparticles morphology

In order to observe the effects of surfactants on the morphologies of the TiO₂ nanoparticles synthesized, their SEM images were compared. Figure 3 shows the SEM image of the TiO₂ nanoparticles (without surfactant); the nanoparticles did not show any particular uniformity, and perhaps were amorphous. In the absence of surfactants, titanium alkoxides strongly react with water, causing amorphous precipitates of TiO₂ nanoparticles [31]. Figure 4 presents the SEM images of the TiO₂ nanoparticles modified with the three different surfactants.

The T/AOT and T/TX100 nanoparticles showed spherical morphologies, however, the T/TX100 nanoparticles appeared to be agglomerated. The T/TBAB nanoparticles manifested a plate-like morphology, while plates were somewhat stuck together. The alteration in morphology of the TiO₂ nanoparticles could be attributed to the surfactants' micelles in the aqueous solution, which inhibit high aggregation of nanoparticles [32].

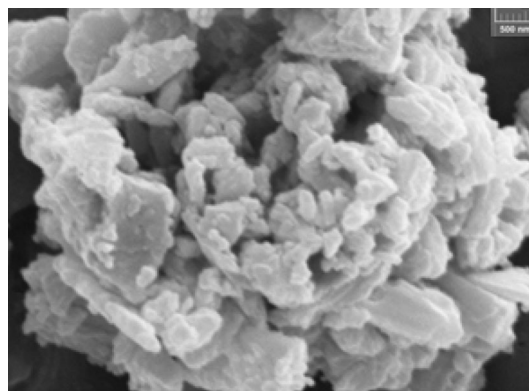


Fig. 3 SEM image of the TiO₂ nanoparticles calcined at 500 °C

5.1.2 Effects of AOT concentration on morphology of TiO₂ nanoparticles

In addition to the type, the surfactant concentration also affected the morphology of the synthesized nanoparticles. Figure 5 shows the SEM images of T/AOT and T/AOT-0.08 nanoparticles. The sample prepared with 0.15 molar concentration of AOT showed agglomeration of the TiO₂

Fig. 4 SEM images of TiO₂ nanoparticles synthesized using different surfactants. **a** T/AOT, **b** T/TX100, and **c** T/TBAB

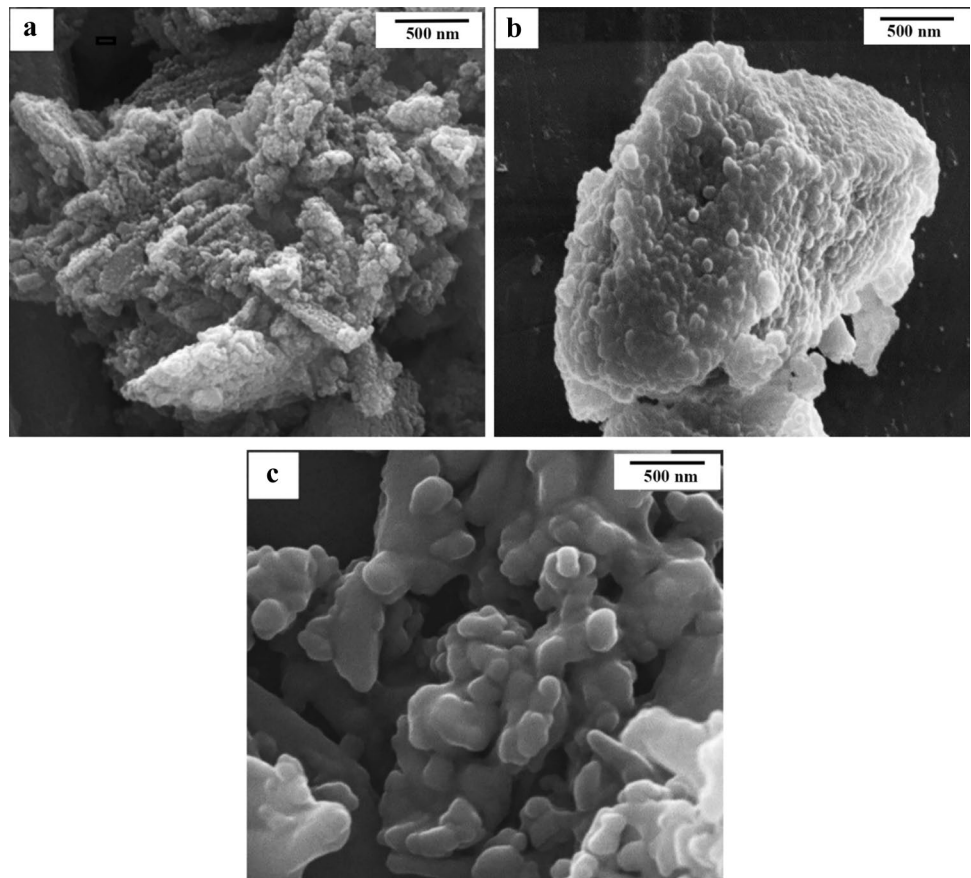
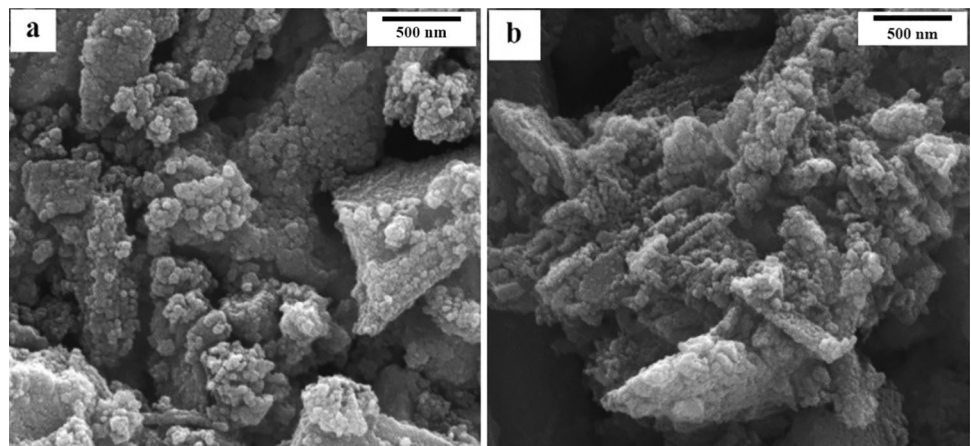


Fig. 5 SEM images of TiO₂ nanoparticles synthesized at two different AOT concentrations. **a** 0.08 molar, and **b** 0.15 molar

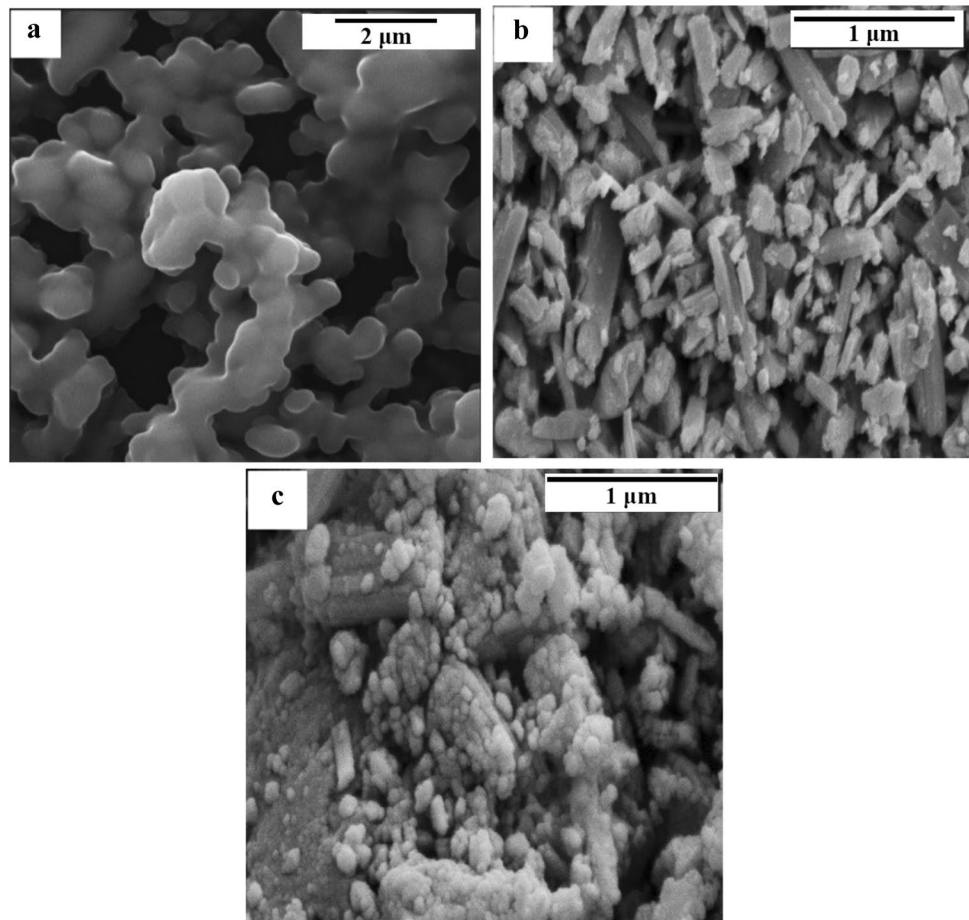


nanoparticles (Fig. 5a), while the sample prepared with 0.08 molar concentration was uniformly spherical in shape and showed less agglomeration (Fig. 5b). As the concentration decreased, so did the size of the agglomerated surfactants in microemulsion, leading to smaller, spherical and uniform particle size of the final product [33]. Therefore, amongst all samples, the one prepared using 0.08 molar concentration of AOT provided the best nanoparticles.

5.1.3 Effects of surfactants on Zr-doped TiO₂ nanoparticles morphology

The effects of surfactants on the synthesis of Zr-doped TiO₂ nanoparticles were also studied. Figure 4 shows the SEM images of the synthesized Zr-doped TiO₂ nanoparticles. As can be observed, the Z/T/AOT nanoparticles shown in Fig. 6a have a layered morphology but the nanoparticles are stuck together. The Z/T/TBAB nanoparticles shown in Fig. 6b have a rod shape morphology but the

Fig. 6 SEM images of Zr-doped TiO₂ nanoparticles synthesized using different surfactants. **a** Z/T/AOT, **b** Z/T/TBAB, and **c** Z/T/TX100



nanoparticles are quite agglomerated. However, when surfactant TX-100 was used, morphology of the Z/T/TX100 nanoparticles became spherical as shown in Fig. 6c. In terms of morphologies, the difference between the Z/T/TX100 nanoparticles and those of the other two samples could be that the Z/T/TX100 nanoparticles formed on the side of micelle layers while the other two samples formed on the side of water pool. Therefore, by comparing the SEM images of the Zr-doped TiO₂ nanoparticles, it was clear that the nanoparticles manifested dissimilar morphologies. Moreover, their morphologies were dissimilar to those of the TiO₂ nanoparticles synthesized using corresponding surfactants.

5.2 Fourier transformed infrared spectroscopy (FTIR)

Figure 7 shows FTIR spectra of the synthesized nanoparticles in the frequency range of 400–4000 cm⁻¹. For all the synthesized nanoparticles, the broad peaks related to the stretching vibration and flexural vibration of OH groups were observed in the ranges of 3300–3500 cm⁻¹ and 1620–1640 cm⁻¹, respectively [34]. The peaks at

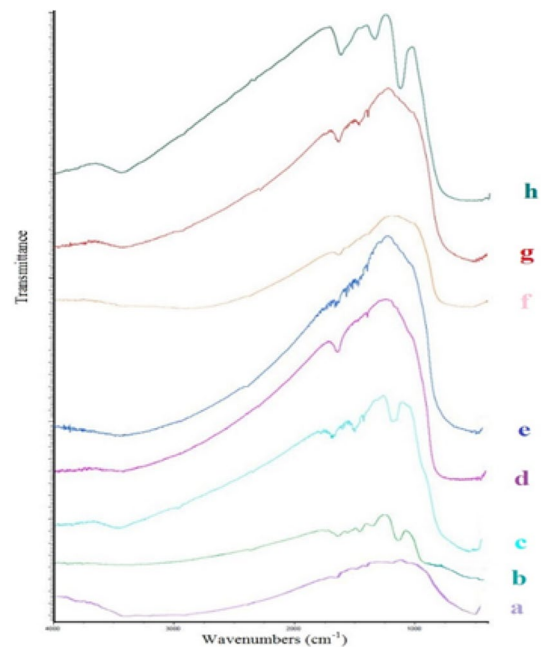


Fig. 7 FTIR spectra of nanoparticles, **a** TiO₂, **b** T/AOT-0.08, **c** T/AOT, **d** T/TX100, **e** T/TBAB, **f** Z/T/TBAB, **g** Z/T/TX100, **h** Z/T/AOT

1000–1300 cm^{-1} for samples b, c, and h are due to the residues of the organic compounds [35]. The lack of peaks for other samples can be ascribed to total removal of the organic compounds during calcination. Moreover, the observed peaks in the region of 400–900 cm^{-1} are related to the vibrations of mineral lattice of Ti–O–Ti for samples b, c, d, and e and those of Zr–O for samples f, g, and h. These results are in agreement with previous findings [36].

5.3 XRD analysis

The XRD patterns for TiO_2 and three modified TiO_2 samples are shown in Fig. 8. In curve (a), which is for TiO_2 sample, the characteristic peaks of the planes (101), (113), (200) and (110) (101), (111) appeared at the 2θ 's of 25.5°, 37.14°, 48.24° and 27.64°, 36.38°, 41.53°, respectively. These results demonstrated a combination of the anatase and rutile phases of TiO_2 , which are in agreement with the standard patterns of [JCPDS 01-1626] and [JCPDS 04-0345], respectively. Curve (b) is the XRD pattern for T/AOT nanoparticles. The characteristic peaks of the planes (101), (112), and (200) appeared at the 2θ 's of 25.44°, 38.11° and 48.17°, respectively, which indicated a pure anatase phase in accord with the standard pattern of [JCPDS 10-0841]. Compared to TiO_2 , the intensity peaks of T/AOT were shorter, which indicated a reduction in the degree of crystallinity. Although the XRD patterns of T/TX100 (curve c) and T/TBAB (curve d) nanoparticles showed pure anatase phase (as was the case with T/AOT) and follow the standard pattern of [JCPDS 10-0841], their intensity peaks were taller, compared to the TiO_2 nanoparticles, which indicated higher degree of crystallinity for these nanoparticles.

Based on the XRD results, it can be said that compared to the TiO_2 nanoparticles, the application of surfactants

caused and facilitated higher degree of crystallinity in the anatase phase.

In Fig. 9, the XRD patterns of the T/AOT and T/AOT-0.08 nanoparticles are shown. As it is obvious from the XRD patterns, the synthesized nanoparticles had crystalline phase of anatase. However, as the concentration of AOT reduced from 0.15 to 0.08 molar, the peaks intensity and degree of crystallinity increased. With the reduction in AOT concentration, no change occurred in the formation of crystalline phase of the nanoparticles, since the crystalline phase formation depends on the calcination temperature; therefore, variations in the concentration of surfactants do not affect the crystalline phase formation, but only the degree of crystallinity. The XRD patterns for T/AOT and T/AOT-0.08 nanoparticles are congruent with the standard pattern of [GCPDS 10-0841].

The XRD patterns of Zr-doped TiO_2 nanoparticles synthesized using different surfactants is given in Fig. 10. For all three samples, and at varying intensities, the characteristic peaks of planes (101), (200), (105), at 2θ 's of 25.22°, 47.9°, 54.2° were due to the presence of anatase crystalline phase of TiO_2 . However, the characteristic peaks of the plane (101) at 2θ of 31.06° showed the tetragonal crystalline phase of TiO_2 . Their XRD patterns are in accord with the standard pattern of [GCPDS 80-1783].

The X-ray diffraction peaks of crystal plane (101) for TiO_2 and three other Zr containing TiO_2 samples are shown in Fig. 11. Compared to the TiO_2 nanoparticles, the peaks for all three Zr containing samples shifted to smaller diffraction angles, indicating larger interplanar spacing due to the presence of Zr in their structures at the substitutional sites [37]. This finding is in agreement with a previous report [38]. Furthermore, the lack of rutile phase peaks

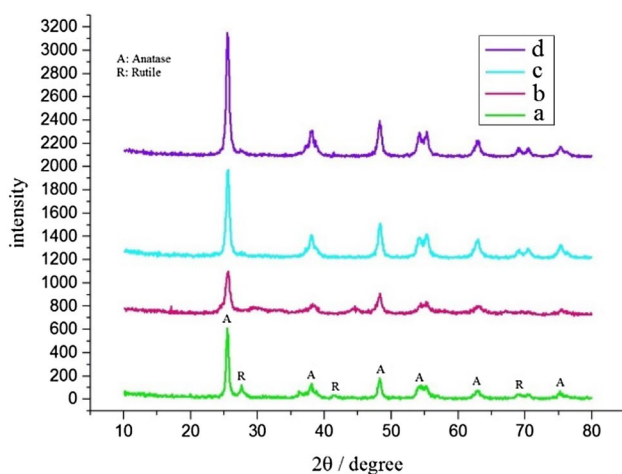


Fig. 8 XRD patterns for TiO_2 and three modified TiO_2 nanoparticles, **a** TiO_2 , **b** T/AOT, **c** T/TX100, and **d** T/TBAB

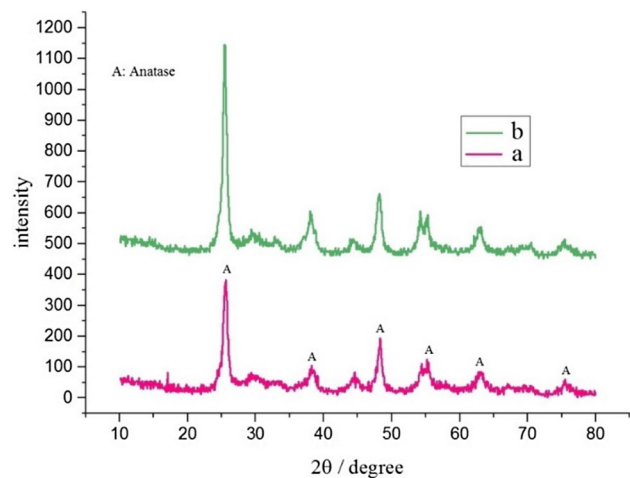


Fig. 9 XRD patterns of TiO_2 nanoparticles synthesized at two different concentrations of AOT surfactant, **a** T/AOT, **b** T/AOT-0.08

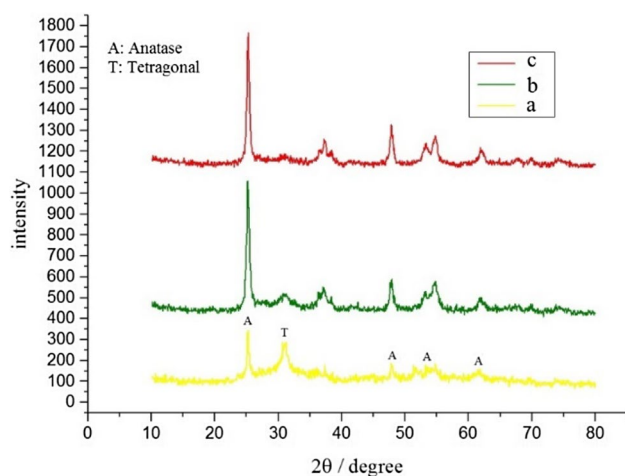


Fig. 10 XRD patterns of Zr-doped TiO₂ nanoparticles synthesized using different surfactants, **a** Z/T/AOT, **b** Z/T/TX100, **c** Z/T/TBAB

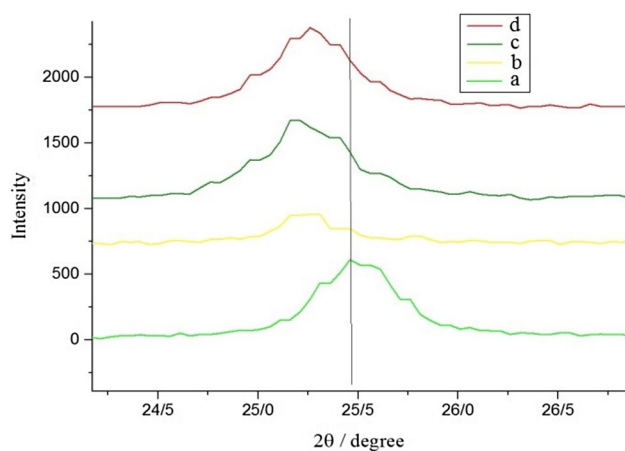


Fig. 11 X-ray diffraction peaks of crystal plane (101), **a** TiO₂, **b** Z/T/AOT, **c** Z/T/TX100, **d** Z/T/TBAB

can be ascribed to the presence of zirconium ions in the structure of these nanoparticles [39].

5.4 EDS analysis

Figure 12 shows the EDS spectra of Zr-doped TiO₂ nanoparticles synthesized using different surfactants in the range of 0.2–4.5 keV [38]. In all three samples, no impurity was observed. It is evident that the Zr doped is evenly scattered on the TiO₂ surface.

5.5 TEM investigation

The best nanoparticles prepared were evaluated using TEM. Figure 13 shows the TEM image of the T/AOT-0.08 nanoparticles as the best sample. The nanoparticles are

quite uniform and have a spherical morphology with size range of 40–50 nm. This observation is in agreement with the results of SEM analysis.

5.6 Evaluation of photocatalytic activity results

Figure 14 shows A reactor was used to investigate the photocatalytic activity of the synthesized nanoparticles in degrading MB dye pollutant. In the reactor, 2 ultraviolet lamps of 15 watts were used as the light source. In order to conduct the dye degradation, the desired amount of catalyst was dispersed in the dye solution at ultrasonic bath for half an hour. Also, in order to keep the adsorption–desorption balanced, the solution was stirred for half an hour in the absence of light. Then, the photocatalytic reaction was carried out under ultraviolet irradiation. During the MB dye degradation process, to facilitate the solution adsorption speed, the dye solution was stirred for all the reaction times. Besides, for constant presence of the oxygen bubbles in the sample solution and for provision of the oxidation conditions, the pipe connected to the aquarium pump was placed in the dye solution. During the reaction procedure, the sampling was carried out for 3 ml using a syringe at a predetermined time. Using the UV–Vis spectroscopy, the amount of remaining dye was estimated in the ultraviolet region. Finally, photocatalytic activities of the synthesized photocatalysts were obtained based on calculation and comparison of their amounts of dye degradation in percentage terms. Percentages of the dye degradation efficiency for these photocatalysts can be calculated using Formula (1):

$$\text{Percentage of dye degradation efficiency} = \frac{C_0 - C_t}{C_0} \times 100 \quad (1)$$

where C_0 is the amount of solution adsorption at zero time and C_t is the amount of solution adsorption at t time.

Figure 15 presents the diagram of MB dye degradation efficiency for all synthesized samples under similar test conditions in 300 min. The MB dye degradation of TiO₂ sample in 300 min is equal to 35%, which is not a considerable percentage (curve a). However, in the same duration of time, an increase was observed in the MB dye degradation percentage for the surfactant modified TiO₂, and also for the Zr-doped TiO₂ nanoparticles. Among the synthesized photocatalysts, the T/AOT-0.08 nanoparticles showed 76% of the MB dye degradation indicating the best performance (curve h). The superior activity of the T/AOT-0.08 nanoparticles can be attributed to their small particle sizes (around 40–50 nm) and more active sites. In view of the aforementioned, it can be suggested that the presence of surfactants and Zr

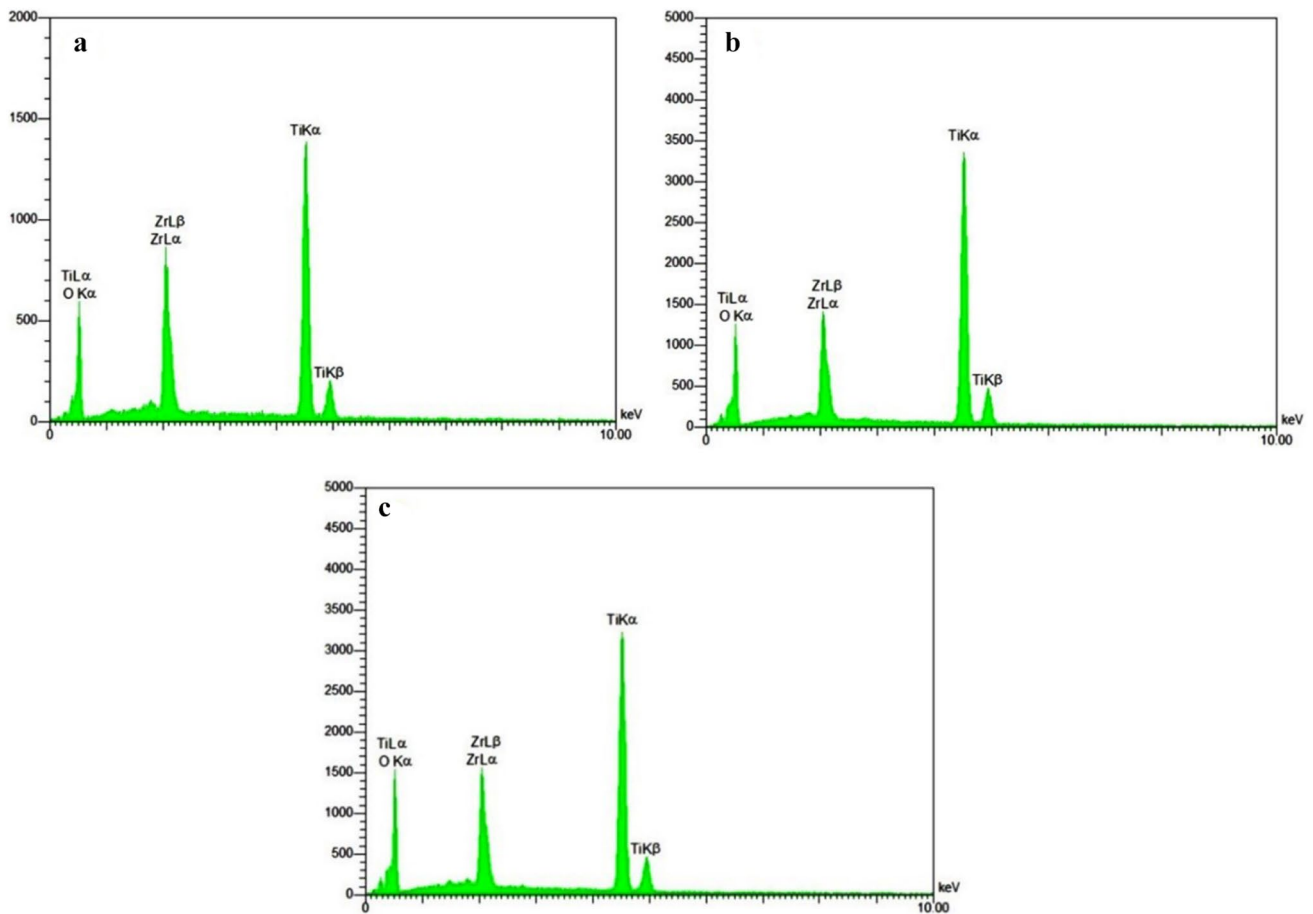


Fig. 12 EDS spectra, **a** Z/T/AOT, **b** Z/T/TBAB, **c** Z/T/TX100

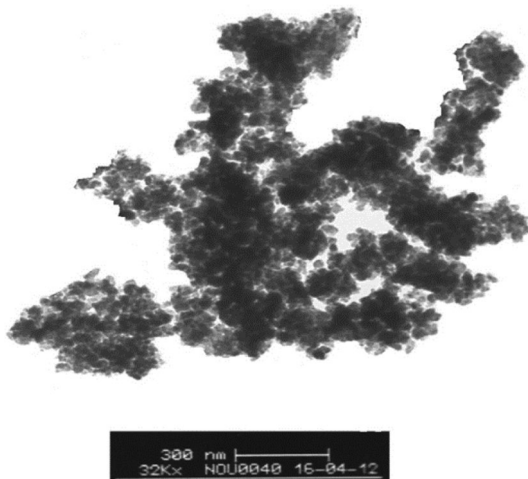


Fig. 13 TEM image of T/AOT-0.08 nanoparticles. They are spherical and in the size range of 40–50 nm

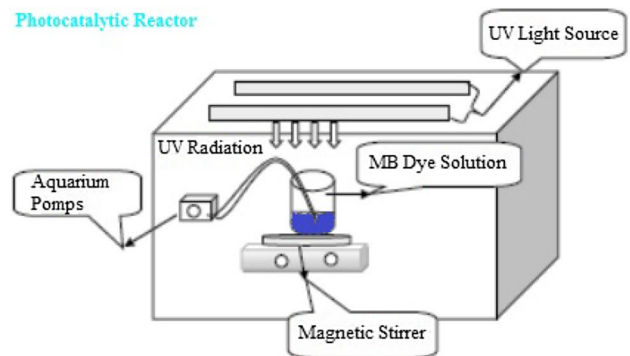


Fig. 14 Schematic illustration of photoreactor designed to perform photocatalytic activity under ultraviolet radiation

in TiO_2 nanoparticles results in the increase of the photocatalytic activities. By trapping the electrons, the Zr ions inhibit the electron-hole pair recombination and improve the photocatalytic activity [40].

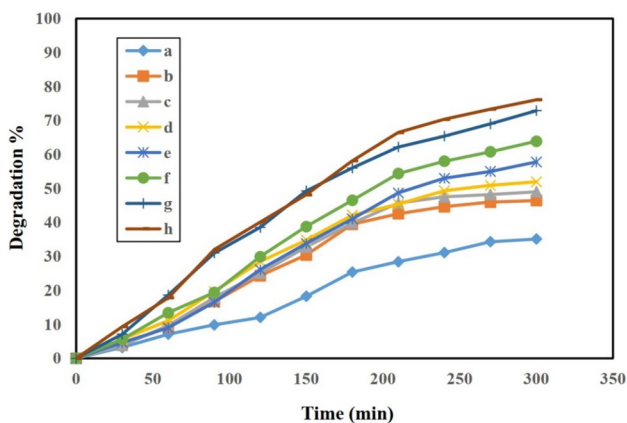


Fig. 15 Diagram of the MB dye degradation efficiency in 300 min for the sample: **a** TiO₂, **b** T/TX100, **c** T/AOT, **d** Z/T/TX100, **e** T/TBAB, **f** Z/T/TBAB, **g** Z/T/AOT, **h** T/AOT-0.08. (photocatalyst amount: 10 mg, initial concentration of the dye solution: 20 ppm, time of ultraviolet irradiation: 300 min, pH = 7, temperature: 25 °C)

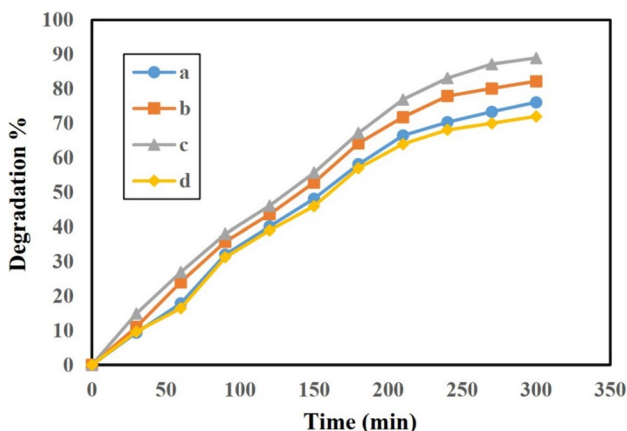


Fig. 16 Effect of T/AOT-0.08 photocatalyst amount on MB dye degradation efficiency: **a** 10 mg, **b** 20 mg, **c** 30 mg, **d** 40 mg. (initial concentration of dye solution: 20 ppm, light irradiation time: 300 min, pH = 7, temperature: 25 °C)

5.6.1 Effects of T/AOT-0.08 amount on MB dye degradation

In Fig. 14, the effect of photocatalyst T/AOT-0.08 amount on the MB dye degradation is drawn. Various amounts (10, 20, 30, and 40 mg) of T/AOT-0.08 photocatalyst were used to investigate its effect on the MB dye degradation. As Fig. 16 shows, with an increase in the amount of photocatalyst from 10 to 30 mg, its photocatalytic efficiency for the MB dye degradation increased from 76 to 89%.

On the other hand, as the T/AOT-0.08 photocatalyst amount increased to 40 mg, its photocatalytic efficiency decreased to 72% (curve d). The increase in the photocatalyst amount resulted in the agglomeration and thus decrease in the surface active sites, and consequently

decreased the MB dye degradation efficiency of the photocatalyst. In view of the aforementioned, it can be suggested that the amount of catalyst has two limiting factors. First, in any amount higher than the optimal amount of photocatalyst, the photocatalytic particles agglomerated in the dye solution, which in turn led to the reduction in the number of surface active sites. Second, beyond the optimal amount of the photocatalyst, light penetration into the solution diminished, consequently causing reduction in the MB dye degradation efficiency of the photocatalyst [2, 41].

5.6.2 Effect of MB dye solution pH

Another influential factor in the photocatalytic activity of nanoparticles is the pH of the dye solution. In all tests, to study the effect of pH, hydrochloric acid (HCl) or sodium hydroxide (NaOH) was used. The effect of dye solution pH on the efficiency of T/AOT-0.08 nanoparticles is presented in Fig. 17. By reducing in the pH of dye solution from 7 to 4, the MB dye degradation efficiency of T/AOT-0.08 nanoparticles decreased from 76 to 60%. However, by increasing the pH to 9, the MB dye degradation efficiency of T/AOT-0.08 nanoparticles increased to 86%. The surface of the nanoparticles in acidic conditions (pH = 4) had a positive load, and a negative load under basic conditions (pH = 9). Therefore, by increasing the pH of dye solution, the number of hydroxyl radicals and subsequently the surface adsorption of the cationic molecules of MB at the surface of the T/AOT-0.08 photocatalyst increased, which resulted in the improvement of photocatalytic activity [42, 43]. However, in the acidic conditions, the surface adsorption of the cationic molecules of MB at the surface of T/AOT-0.08 photocatalyst decreased and subsequently the MB dye degradation efficiency decreased [44].

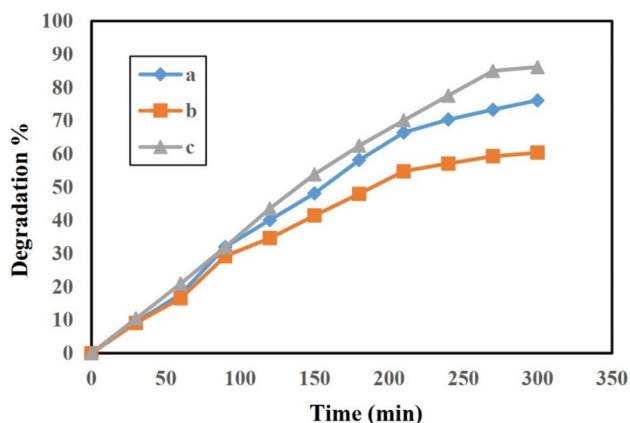


Fig. 17 Effect of MB dye solution pH on photocatalytic degradation efficiency of T/AOT-0.08: **a** 7, **b** 4, **c** 9 (photocatalyst amount: 10 mg, initial concentration of solution: 20 ppm, temperature: 25 °C)

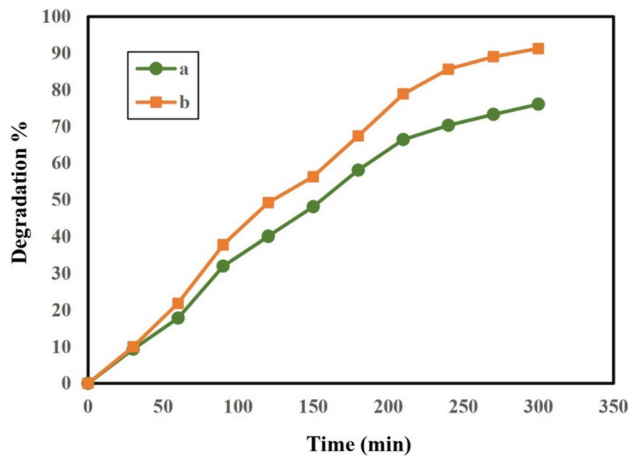


Fig. 18 Effect of MB dye solution temperature on photocatalytic efficiency of T/AOT-0.08 nanoparticles: **a** 25 °C, **b** 50 °C (photocatalyst amount: 10 mg, initial concentration of the dye solution: 20 ppm, pH=7)

5.6.3 Effect of MB dye solution temperature

Figure 18 shows the effect of MB dye solution temperature on the photocatalytic efficiency of T/AOT-0.08 nanoparticles. The reaction was first conducted at a temperature of 25 °C, and then at 50 °C while all other parameters were kept constant. As the results showed, by increasing temperature, the MB dye degradation efficiency of T/AOT-0.08 photocatalyst increased from 76 to 91%. Therefore, it can be understood that at the higher temperature, formation of bubbles and production of free radicals in the dye solution occurred. Besides, the increased temperature lessened the possibility of electron-hole pair recombination, and thus the dye degradation efficiency of the photocatalyst increased [45].

6 Conclusion

In this study, 8 samples were synthesized in the presence of various surfactants using microemulsion method. Based on the XRD results, it was found that the presence of surfactants affected the formation of pure anatase phase of TiO₂ nanoparticles. Moreover, it was found that not only the type but also the concentration of surfactants affected the morphology of the synthesized nanoparticles. After preparation and characterization of the nanoparticles, the pollutant MB dye was used to evaluate their photocatalytic efficiency. The T/AOT-0.08 sample was found to be the best photocatalyst due to its uniform spherical morphology and particle sizes of 40-50 nm, dye degradation efficiency of 76% at 25 °C, and 91% at 50 °C.

Compliance with ethical standards

Conflict of interest The authors declare that they have no conflict of interest.

References

1. Byrappa K, Subramani A, Ananda S, Rai KL, Dinesh R, Yoshimura M (2006) Photocatalytic degradation of rhodamine B dye using hydrothermally synthesized ZnO. *Bull Mater Sci* 29(5):433–438
2. Prabhakarao N, Chandra MR, Rao TS (2017) Compounds, Synthesis of Zr doped TiO₂/reduced Graphene Oxide (rGO) nanocomposite material for efficient photocatalytic degradation of Eosin Blue dye under visible light irradiation. *J Alloy Compd* 694:596–606
3. Durga M, Bharathi S, Murthy PB, Devasena T (2015) Characterization and phytotoxicity studies of suspended particulate matter (SPM) in Chennai urban area. *J Environ Biol* 36(3):583
4. Abazari R, Mahjoub AR, Sanati SA (2014) A facile and efficient preparation of anatase titania nanoparticles in micelle nano-reactors: morphology, structure, and their high photocatalytic activity under UV light illumination. *RSC Adv* 4(99):56406–56414
5. Mohamed IM, Dao V-D, Barakat NA, Yasin AS, Yousef A, Choi H-S (2016) Efficiency enhancement of dye-sensitized solar cells by use of ZrO₂-doped TiO₂ nanofibers photoanode. *J Colloid Interface Sci* 476:9–19
6. Braun JH, Baidins A, Marganski RE (1992) TiO₂ pigment technology: a review. *Prog Org Coat* 20(2):105–138
7. Pfaff G, Reynders P (1999) Angle-dependent optical effects deriving from submicron structures of films and pigments. *Chem Rev* 99(7):1963–1982
8. Mai F, Lu C, Wu C, Huang C, Chen J, Chen C (2008) Technology, mechanisms of photocatalytic degradation of victoria blue R using nano-TiO₂. *Sep Purif Technol* 62(2):423–436
9. Ba-Abbad MM, Kadhum AAH, Mohamad AB, Takriff MS, Sopian K (2012) Synthesis and catalytic activity of TiO₂ nanoparticles for photochemical oxidation of concentrated chlorophenols under direct solar radiation. *Int J Electrochem Sci* 7(6):4871–4888
10. Anderson A-L, Binions RJP (2015) The effect of Brij® surfactants in sol-gel processing for the production of TiO₂ thin films. *Polyhedron* 85:83–92
11. Pelaez M, Nolan NT, Pillai SC, Seery MK, Falaras P, Kontos AG, Dunlop PS, Hamilton JW, Byrne JA, O'shea K (2012) A review on the visible light active titanium dioxide photocatalysts for environmental applications. *Appl Catal B* 125:331–349
12. Daghri R, Droguai P, Robert D (2013) Modified TiO₂ for environmental photocatalytic applications: a review. *Ind Eng Chem Res* 52(10):3581–3599
13. Liao D, Badour C, Liao B (2008) Preparation of nanosized TiO₂/ZnO composite catalyst and its photocatalytic activity for degradation of methyl orange. *J Photochem Photobiol A* 194(1):11–19
14. Sobana N, Selvam K, Swaminathan M (2008) Optimization of photocatalytic degradation conditions of Direct Red 23 using nano-Ag doped TiO₂. *Sep Purif Technol* 62(3):648–653
15. Wu Y, Zhang J, Xiao L, Chen F (2009) Preparation and characterization of TiO₂ photocatalysts by Fe³⁺ doping together with Au deposition for the degradation of organic pollutants. *Appl Catal B* 88(3–4):525–532
16. Wang X, Lim T-T (2013) Highly efficient and stable Ag–AgBr/TiO₂ composites for destruction of Escherichia coli under visible light irradiation. *Water Res* 47(12):4148–4158
17. Li G, Dimitrijevic NM, Chen L, Rajh T, Gray KA (2008) Role of surface/interfacial Cu²⁺ sites in the photocatalytic

- activity of coupled CuO–TiO₂ nanocomposites. *J Phys Chem C* 112(48):19040–19044
18. Gnanasekaran L, Hemamalini R, Saravanan R, Ravichandran K, Gracia F, Gupta VK (2016) Intermediate state created by dopant ions (Mn, Co and Zr) into TiO₂ nanoparticles for degradation of dyes under visible light. *J Mol Liq* 223:652–659
 19. Kruefu V, Ninsonti H, Wetchakun N, Inceesungvorn B, Pookmanee P, Phanichphant S (2012) Photocatalytic degradation of phenol using Nb-loaded ZnO nanoparticles. *Eng J* 16(3):91–100
 20. Sinirtas E, Sleyen M, Soyul GS (2016) Photocatalytic degradation of 2, 4-dichlorophenol with V₂O₅-TiO₂ catalysts: effect of catalyst support and surfactant additives. *Chin J Catal* 37(4):607–615
 21. Chen K, Li J, Wang W, Zhang Y, Wang X, Su H (2012) Effects of surfactants on microstructure and photocatalytic activity of TiO₂ nanoparticles prepared by the hydrothermal method. *Mater Sci Semicond Process* 15(1):20–26
 22. Linsebigler AL, Lu G, Yates JT Jr (1995) Photocatalysis on TiO₂ surfaces: principles, mechanisms, and selected results. *Chem Rev* 95(3):735–758
 23. Mbiri A, Taffa DH, Gatebe E, Wark M (2019) Zirconium doped mesoporous TiO₂ multilayer thin films: influence of the zirconium content on the photodegradation of organic pollutants. *Catal Today* 328:71–78
 24. Fu C, Gong Y, Wu Y, Liu J, Zhang Z, Li C, Niu L (2016) Photocatalytic enhancement of TiO₂ by B and Zr co-doping and modulation of microstructure. *Appl Surf Sci* 379:83–90
 25. Hirano M, Nakahara C, Ota K, Tanaike O, Inagaki M (2003) Photoactivity and phase stability of ZrO₂-doped anatase-type TiO₂ directly formed as nanometer-sized particles by hydrolysis under hydrothermal conditions. *J Solid State Chem* 170(1):39–47
 26. Mao L, Li Q, Dang H, Zhang Z (2005) Synthesis of nanocrystalline TiO₂ with high photoactivity and large specific surface area by sol–gel method. *Mater Res Bull* 40(2):201–208
 27. Bian Z, Zhu J, Cao F, Huo Y, Lu Y, Li H (2010) Solvothermal synthesis of well-defined TiO₂ mesoporous nanotubes with enhanced photocatalytic activity. *Chem Commun* 46(44):8451–8453
 28. Gandhi V, Mishra M, Rao M, Kumar A, Joshi P, Shah D (2011) Comparative study on nano-crystalline titanium dioxide catalyzed photocatalytic degradation of aromatic carboxylic acids in aqueous medium. *J Ind Eng Chem* 17(2):331–339
 29. Lee MS, Lee G-D, Ju C-S, Hong S-S (2005) Preparations of nano-sized TiO₂ in reverse microemulsion and their photocatalytic activity. *Sol Energy Mater Sol Cells* 88(4):389–401
 30. Kronberg B, Lindman B (2003) Surfactants and polymers in aqueous solution. Wiley, Chichester
 31. Sanchez-Dominguez M, Pemartin K, Boutonnet M (2012) Preparation of inorganic nanoparticles in oil-in-water microemulsions: a soft and versatile approach. *Curr Opin Colloid Interface Sci* 17(5):297–305
 32. Liao D, Liao B (2007) Effects of surfactant composition and concentration on shape, size and photocatalytic activity of TiO₂ nanoparticles. *Int J Chem React Eng* 5(1):1–15
 33. Pileni M (1993) Reverse micelles as microreactors. *J Phys Chem* 97(27):6961–6973
 34. Wu J-M, Shih HC, Wu W-T, Tseng Y-K, Chen I-C (2005) Thermal evaporation growth and the luminescence property of TiO₂ nanowires. *J Cryst Growth* 281(2–4):384–390
 35. Wang YM, Liu SW, Lü MK, Wang SF, Gu F, Gai XZ, Cui XP, Pan J (2004) Preparation and photocatalytic properties of Zr⁴⁺-doped TiO₂ nanocrystals. *J Mol Catal A Chem* 215(1–2):137–142
 36. Shao GN, Imran S, Jeon SJ, Engole M, Abbas N, Haider MS, Kang SJ, Kim HT (2014) Sol–gel synthesis of photoactive zirconia–titania from metal salts and investigation of their photocatalytic properties in the photodegradation of methylene blue. *Powder Technol* 258:99–109
 37. Wang J, Yu Y, Li S, Guo L, Wang E, Cao Y (2013) Doping behavior of Zr⁴⁺ ions in Zr⁴⁺-doped TiO₂ nanoparticles. *J Phys Chem C* 117(51):27120–27126
 38. Venkatachalam N, Palanichamy M, Arabindoo B, Murugesan V (2007) Enhanced photocatalytic degradation of 4-chlorophenol by Zr⁴⁺ doped nano TiO₂. *J Phys Chem C* 266(1–2):158–165
 39. Eskandarloo H, Badieli A, Behnajady MA (2014) Study of the effect of additives on the photocatalytic degradation of a triphenylmethane dye in the presence of immobilized TiO₂/NiO nanoparticles: artificial neural network modeling. *Ind Eng Chem Res* 53(17):6881–6895
 40. Neppolian B, Wang Q, Yamashita H, Choi H (2007) Synthesis and characterization of ZrO₂-TiO₂ binary oxide semiconductor nanoparticles: application and interparticle electron transfer process. *Appl Catal A* 333(2):264–271
 41. Saquib M, Tariq MA, Haque M, Muneer M (2008) Photocatalytic degradation of disperse blue 1 using UV/TiO₂/H₂O₂ process. *J Environ Manag* 88(2):300–306
 42. Chiang Y-J, Lin C-C (2013) Photocatalytic decolorization of methylene blue in aqueous solutions using coupled ZnO/SnO₂ photocatalysts. *Powder Technol* 246:137–143
 43. Gao B, Lim TM, Subagio DP, Lim T-T (2010) Zr-doped TiO₂ for enhanced photocatalytic degradation of bisphenol A. *Appl Catal A* 375(1):107–115
 44. Pouretedal HR, Norozi A, Keshavarz MH, Semnani A (2009) Nanoparticles of zinc sulfide doped with manganese, nickel and copper as nanophotocatalyst in the degradation of organic dyes. *J Hazard Mater* 162(2–3):674–681
 45. Karimi L, Zohoori S, Yazdanshenas ME (2014) Photocatalytic degradation of azo dyes in aqueous solutions under UV irradiation using nano-strontium titanate as the nanophotocatalyst. *J Saudi Chem Soc* 18(5):581–588

Publisher's Note Springer Nature remains neutral with regard to jurisdictional claims in published maps and institutional affiliations.